

Transitions in the Horizontal Transport of Vertically Vibrated Granular Layers

Z. Farkas, P. Tegzes, A. Vukics, and T. Vicsek

Department of Biological Physics, Eötvös University, Budapest, Pázmány P. Sztv. 1A, 1117 Hungary

(October 17, 2019)

Motivated by recent advances in the investigation of fluctuation-driven ratchets and flows in excited granular media, we have carried out experimental and simulational studies to explore the horizontal transport of granular particles in a vertically vibrated system whose base has a sawtooth-shaped profile. The resulting material flow exhibits novel collective behavior, both as a function of the number of layers of particles and the driving frequency; in particular, under certain conditions, increasing the layer thickness leads to a *reversal of the current*, while the onset of transport as a function of frequency can occur either *gradually or suddenly* in a manner reminiscent of a phase transition. Our new and previous experimental findings are interpreted here with the help of extensive, event driven Molecular Dynamics simulations. In addition to reproducing the experimental results, the simulations revealed that the current may be *reversed* as a function of the *driving frequency* as well. We also give details about the simulations so that similar numerical studies could be carried out in a more straightforward manner in the future.

I. INTRODUCTION

The best known and most common transport mechanisms involve gradients of external fields or chemical potentials that extend over the distance traveled by the moving objects. However, recent theoretical studies have shown that there are processes in far from equilibrium systems possessing vectorial symmetry that can bias thermal noise type fluctuations and induce macroscopic motion on the basis of purely local effects. This mechanism is expected to be essential for the operation of molecular combustion motors responsible for many kinds of biological motion; it has also been demonstrated experimentally in simple physical systems [1,2], indicating that it could lead to new technological developments such as nanoscale devices or novel types of particle separators. Motivated by both of these possibilities, as well as by interesting new results for flows in excited granular materials [3–8], we have carried out a series of experimental and simulational studies that explore the manner in which granular particles are *horizontally* transported by means of *vertical* vibration.

In the corresponding theoretical models – known as “thermal ratchets” – fluctuation-driven transport phenomena can be interpreted in terms of overdamped Brownian particles moving through a periodic but asymmetric, one-dimensional potential in the presence of nonequilibrium fluctuations [9–12]. Typically, a sawtooth-shaped potential is considered, and the nonlinear fluctuations are represented either by additional random forces or by switching between two different potentials. Collective effects occurring during the fluctuation-driven motion have also been considered [13–15], leading to a number of unusual effects that include current reversal as a function of particle density. Here we investigate an analogous transport mechanism for granular materials. By carrying out

experiments – both real and numerical – on granular materials vibrated vertically by a base with a sawtooth profile, it is possible to achieve a fascinating combination of two topics of considerable current interest – ratchets and granular flows. A number of recent papers have focused on vibration-driven granular flow, and the details of the resulting convection patterns have been examined, both by direct observation [4,5,7,8] and by magnetic resonance imaging [6,16]. Granular convection has also been simulated numerically by several groups; the study most closely related to the present work deals with the horizontal transport that occurs when the base is forced to vibrate in an asymmetric manner [17].

II. EXPERIMENTS

We have experimentally investigated of the horizontal flow of granular material confined between two upright concentric cylinders undergoing vertical vibration. In order to induce transport, the height of the annular base between the cylinders has a periodic, piecewise-linear profile (in other words, it is sawtooth-like). The experimental setup is also described in Ref. [18], and is briefly reviewed here.

A. Apparatus

Figure 1 shows a schematic view of the experimental apparatus. To achieve a quasi-two-dimensional system without boundaries in the direction of the expected flow the granular material is placed between two concentric glass cylinders [7]. The mean diameter of the cylinders is 10 cm, while the gap between the cylinders is either 3 or 5 mm. A ring filling the gap between the cylinders, with

a sawtooth profile on its upper surface, is mounted on the base of the container; the ring is made of either PVC (“soft”), aluminum or CF_4 (“hard”), and different sawtooth shapes are used. The entire assembly is vertically vibrated with a displacement that depends sinusoidally on time.

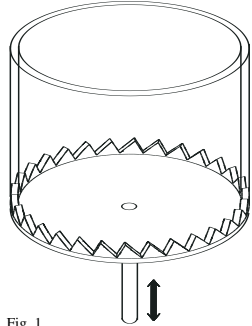


Fig. 1

FIG. 1. The schematic view of the experimental apparatus.

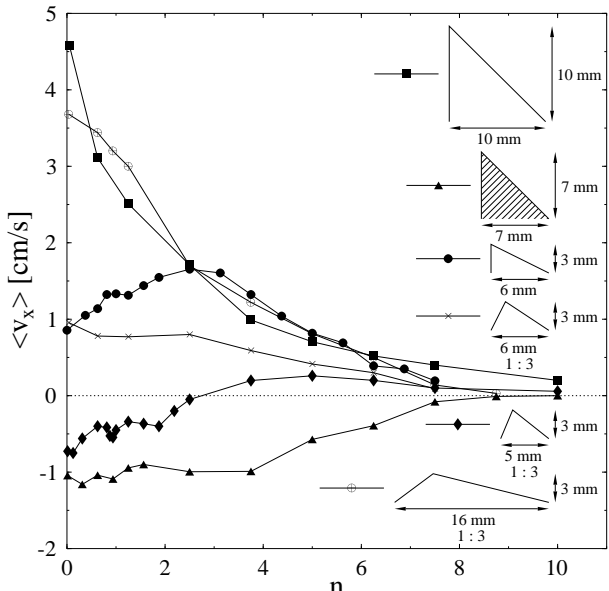


FIG. 2. The average horizontal velocity of the beads as a function of height of the granular layer. Here we characterize the height of the layer by $n = N/k$, where N is the total number of particles and k is the number of particles in a single layer. The various curves represent measurements for various sawtooth shapes (given by their width w , height h , and asymmetry parameter a , which is the ratio of the horizontal projection of the left part of a tooth to its total extension) and materials. The shape of the sawteeth can be seen in the figure, the filled sawtooth represents hard plastic material, the others are made of PVC (soft plastic). The particles are glass balls. The amplitude and the frequency are $A = 2$ mm, $f = 25$ Hz.

Monodisperse glass balls are used in the experiments, which are nearly spherical with diameter $3.3 \text{ mm} \pm 2\%$. As shown in the inset of Fig. 2, the size of the sawteeth

is in the same range as that of the particles.

B. Results

Provided the frequency is sufficiently large, the vertical vibration causes horizontal flow of the entire granular layer. This bulk motion is reproducible over repeated experiments. The average flow velocity is determined by tracking individual tracer particles visible through the transparent cylinder walls. In order to average out fluctuations, the particles are allowed to travel large distances; depending on the size of the fluctuations this distance is between 1.5 and 6 m (equal to 5–20 times the circumference of the system). Each point shown in the graphs is an average over 3–6 tracer particles.

Figure 2 shows the horizontal flow velocity as a function of the number of particles for various possible systems. The actual sawtooth and particle shapes are also indicated. *Positive velocities* are defined as follows: Moving in the positive direction the first edge of a sawtooth is the steeper one; i.e., *from left to the right* for these cases. The vibration amplitude and frequency are $A = 2$ mm and $f = 25$ Hz; the dimensionless acceleration $\Gamma = (2\pi f)^2 A/g$ is an important quantity for vibrated granular systems, so that here $\Gamma = 5$.

We have observed a variety of qualitatively different kinds of behavior, some of which can be interpreted by simple geometrical arguments. The most surprising phenomenon is that in certain cases the velocity changes sign; in other words, the flow *direction* depends on the layer thickness. In some cases the curves are monotonically decreasing, while others have well defined maxima. Altering the particle shape reduces the velocity and shifts the location of the maximum, but the shape of the curve remains unchanged (results not shown here). Likewise, changing the elasticity of the base does not alter the curves qualitatively. The only feature common to the different curves is that beyond a certain layer thickness the velocity magnitude decreases as further layers are added.

Figure 3 shows the Γ dependence of the flow velocity for a system of 200 balls (amounting to 4 layers) for constant A . Flow occurs only above a critical acceleration $\Gamma_c \simeq 1.7$. Above this critical value the velocity appears to follow a power law

$$v(\Gamma) \propto (\Gamma - \Gamma_c)^{0.48}, \quad (1)$$

suggesting that the onset of flow resembles the kind of phase transition observed in hydrodynamic instabilities such as thermal convection [19]. In this particular case the exponent we obtained is close to 1/2 indicating that the transition is more like a bifurcation. However, for other parameters (see, e.g., the simulational results presented in section IV) we obtained other exponents as well.

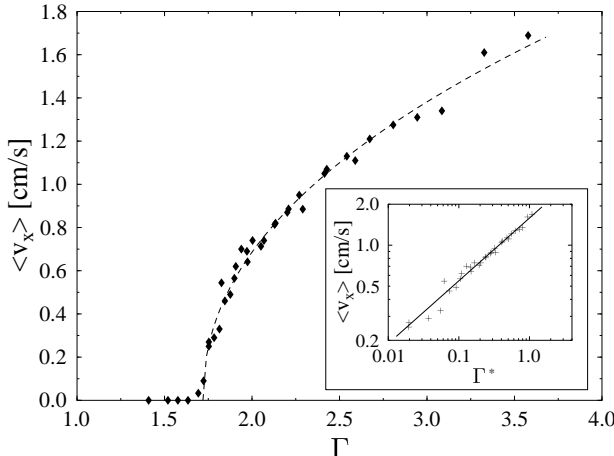


FIG. 3. Horizontal velocity $\langle v_x \rangle$ as a function of the dimensionless acceleration Γ at constant amplitude ($A = 2$ mm). The experiment is for a strongly asymmetric aluminum sawtooth ($w = 12$ mm, $h = 7$ mm, $a = 0$) and 200 glass balls. In the inset we display the data on a log-log scale for $\langle v_x \rangle$ close to the transition as a function of $\Gamma^* = (\Gamma - \Gamma_c)/\Gamma_c$ where $\Gamma_c = 1.7$. The slope of the fitted line is 0.48.

III. EVENT DRIVEN SIMULATIONS

Simulations have been useful in the studies of granular systems [20,21]. Here we perform event driven simulations of inelastic particles with an additional shear friction in a two-dimensional system whose base has a sawtooth-shaped profile. In event driven simulations the difficult part of the algorithm is determining the next event (e.g., the next collision), and the motion of the particles is calculated analytically between two events [24,25]. Since we have not found in the literature a detailed description of the related simulations, here (see Appendix A and B) we give some details of the calculations so that similar studies could be carried out or reproduced in the future in a more direct manner. The event driven simulations discussed below represent an alternative to the more common Molecular Dynamics calculations assuming differentiable interaction potentials between the particles [26].

The particles are modeled as disks with a given radius r_i . These disks can rotate, their moment of inertia is $\frac{1}{2}m_i r_i^2$ (m_i is the mass of the i th particle). The motion of the beads is simulated in two-dimensional cell (see Fig. 4). To realize the topology of the experiment, periodical boundary condition is applied in the horizontal direction. The height of the cell is chosen in such a way that the number of particles hitting the upper wall is negligible. The base is oscillating sinusoidally with frequency f and amplitude A . The geometry of the base can be seen in Fig. 5 in detail. The shape of a tooth can be described by three parameters: its height h , width w and asymmetry parameter a . This asymmetry parameter is $a = l/w$,

where l is the distance of the projection of the sawtooth's top point from the left side point of the unit. The top point of a tooth is rounded by an arc which smoothly joins the two sides.

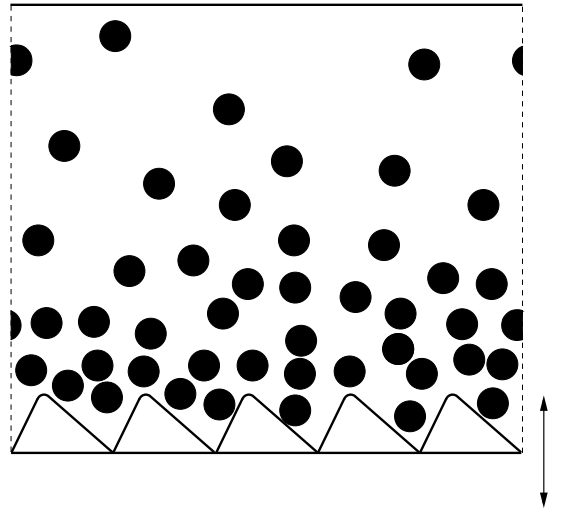


FIG. 4. Visualization of the arrangement used in the simulations. The upper wall is fixed, the sawtooth shaped base is oscillating sinusoidally. Periodic boundary condition is applied in horizontal direction.

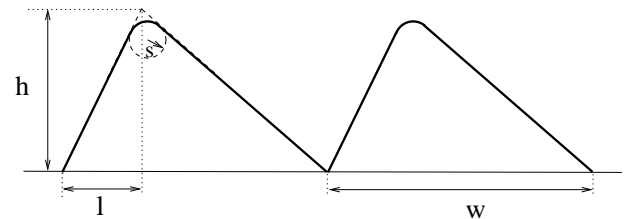


FIG. 5. The geometry of the sawtooth base. The shape of a tooth can be described by three parameters: its height h , width w , and asymmetry parameter $a = l/w$, where l is the horizontal projection of the left part of the tooth. The top of the teeth are rounded by an arc with radius s smoothly joining to both sides.

We consider collisions during which the particles can stick to or slide along each other's surface. The details of the calculating the velocities of two particles after a collision are given in Appendix A.

Furthermore, there are several types of collisions which have to be taken into account as separate cases when the position of the next event is to be determined. These details are described in Appendix B.

Now we give a brief summary of the algorithm and procedures used in the simulations. After a collision, the time of the next collision has to be determined. A simplistic way to do this would be to recalculate the times of all possible collisions. However, this is not necessary for most of the particles, as only (one or two) particles taking part in the last collision change their velocities, so

the time of the last collision can be stored, and is valid until one of the particles collides with another object. Furthermore, in most cases it is not necessary to calculate the time of collision between particles which are far from each other, as it is likely that at least one of them will collide with another object until they would collide.

One possible solution is the following: the simulation space is covered by a grid of spacing $d > 2R_{max}$, where R_{max} is the radius of the biggest particle. Therefore, collisions only between particles (or particle and other object) in neighboring boxes have to be calculated. From this point of view, a particle is in the box where its center is, an object (segment or circle) is in all boxes it covers even partially during its oscillation (if it oscillates). We determine in which box a particle is by introducing the event of a particle leaving a box and entering another one. This method considerably speeds up the algorithm.

However, there remains a further problem typical for event driven granular simulations called inelastic collapse [27]. One possibility to avoid the numerical difficulties associated with it is to make ε_n velocity dependent [27,28]. We use a very simple rule in our simulation. The coefficient of restitution ε is constant until $v'_n > v_n^{min}$ (v'_n is the relative normal velocity of the colliding particles after the collision), however, if v'_n would be less than v_n^{min} , it is set to this minimal normal velocity: $v'_n = v_n^{min}$. Therefore, the relative normal velocity cannot be less than v_n^{min} between two objects after their collision. Using $v_n^{min} = 5$ mm/s is enough to avoid inelastic collapse, and still this extra rule does not influence the dynamics of the system. The simulation program was written in C programming language, and it ran on personal computers with Linux operating system.

IV. RESULTS

The system we studied is a complex one, with many parameters. Since it is impossible to explore the dependence of its behavior on each of the parameters, some of them were fixed in all of the simulations. (Still there remained quite a few parameters to vary, the results shown in this section are selected from simulations with more than 5000 different parameter sets.) We fixed two parameters: the width of a sawtooth was $w = 6$ mm and the amplitude of the oscillation was $A = 2$ mm. According to previous results [29], the *direction* of the horizontal transport does not depend very much on the coefficient of restitution ε and the friction coefficient μ , only its efficiency is lower with higher dissipation. Therefore, we set the dissipation relatively low by using $\varepsilon = 0.8$ and $\mu = 0.1$ between all objects (particle-particle, particle-wall). The radii of the particles varied from 1.05 mm to 1.155 mm uniformly, to avoid the formation of a hexagonal structure which often appears in two dimensions when the system freezes. The masses were equal, hence it did not matter what their actual value was.

A. Dependence on the sawtooth shape

First we investigated how $\langle v_x \rangle$ depends on the shape of the sawtooth (other parameters were kept fixed), where the average has been taken over both time and the individual particles. We intended to find sawtooth shapes resulting in negative transport. According to the experiments, negative transport occurs only for a few particle layers ($n = 0 \dots 3$), and as the number of particles is increased, the direction of the transport becomes positive. We chose $n = 1$, and the frequency was $f = 25$ Hz ($\Gamma = 5.0$). The width of the cell was $24w = 144$ mm, therefore one layer contained about 70 particles. These simulations lasted for 50 internal seconds, the following results represent averages of two runs for each parameter sets (with different initial conditions).

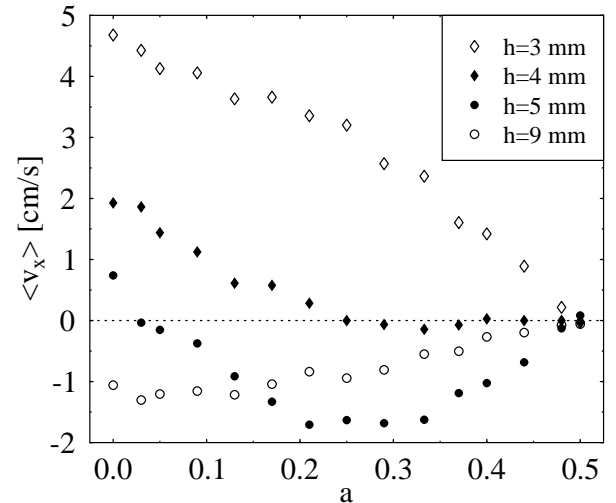


FIG. 6. The horizontal transport as a function of the asymmetry of the sawtooth. The shape of the curves depends on the height h of the sawteeth.

In Fig. 6 $\langle v_x \rangle$ can be seen vs. a (the height was fixed at four different values). The first thing worth to note is that $\langle v_x \rangle$ tends to zero as the shape becomes symmetrical (i. e. a tends to 0.5). The shape of the plots depends on the height h of the sawteeth. At $h = 3$ mm the velocity is positive and decreases monotonically, while at $h = 5$ mm it is negative and has a minimum at $a \simeq 0.25$, and when the height is 9 mm, it is still negative but monotonically increasing. These curves are helpful in understanding the mechanism of negative transport.

In Fig. 7 the dependence of the horizontal transport on the height of the sawteeth can be seen. The shapes of the graphs are similar in case of $a = 0.05$ and $a = 0.333$: $\langle v_x \rangle$ is positive if h is small, and decreases and turns to negative with increasing h . Finally, it becomes zero for high h values. More detailed investigations showed that it is true for nearly all possible values of a (except

for $a \simeq 0.5$, since then the transport vanishes). In conclusion, the horizontal transport can be negative if the height of the sawtooth is between 4 and 16 mm and if the asymmetry parameter a is less than about 0.4. In other cases it is positive or zero (if the sawtooth is symmetric). It is important to note that these results are valid only for a small number of particles. As it will be shown, increasing the number of particles the negative transport vanishes and turns into positive in all cases.

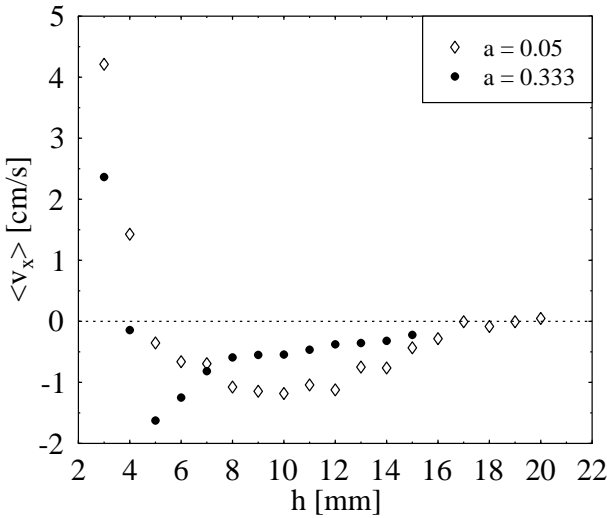


FIG. 7. Horizontal transport as a function of height of the sawtooth. The shape does not depend very much on the asymmetry of the sawtooth.

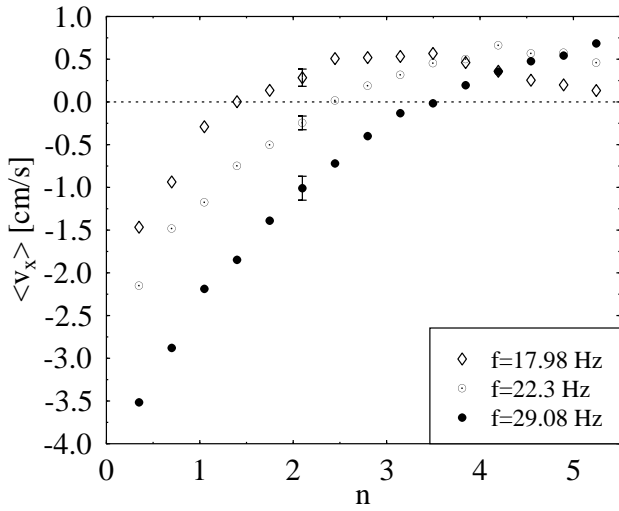


FIG. 8. The horizontal transport as a function of layer width at three different frequencies, when the shape of the sawtooth is: $h = 6$ mm and $a = 0.25$. The system width was $10w = 60$ mm, one run lasted for 30 internal seconds. The data is average of 7 runs.

B. Dependence on the layer width

The results in the previous section show that if there are only few particles, then depending on the shape of a sawtooth, the transport can be negative or positive. Now we show what happens if more and more particles are added into the system.

In Fig. 8 one can see that negative transport becomes zero and turns to positive as the layer width is increased. (Unfortunately the event-driven simulation becomes unfeasible as the density increases with increasing particle number, therefore $n \simeq 5$ is the maximum layer width we can have in our simulation.) If the sawtooth shape is such that even for a few particles the transport is positive, then with increasing particle number the transport decreases (see Fig. 9).

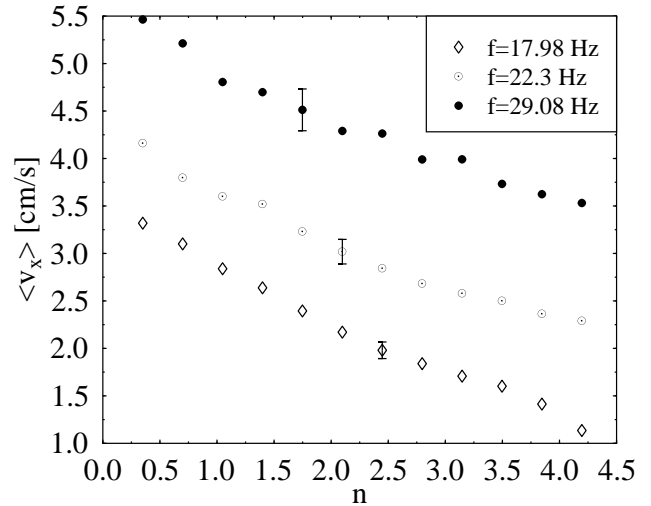


FIG. 9. The horizontal transport as a function of layer width at three different frequencies. The shape of the sawtooth: $h = 3$ mm and $a = 0.1$. The data shown here is average of 7 runs, one run lasted for 30 internal seconds.

C. Frequency dependence

Another interesting question is what happens if the frequency is varied. A sawtooth shape producing negative transport for few particles was chosen. Then with different layer widths the horizontal transport shows interesting behavior as a function of frequency. The results are shown in Fig. 10.

Generally, the negative transport becomes stronger with increasing frequency. In three cases ($n = 1.05$, $n = 1.75$, and $n = 2.8$) the transport *reverses*, from positive to negative. This phenomenon is again very illuminating when we try to explain the mechanism of negative transport.

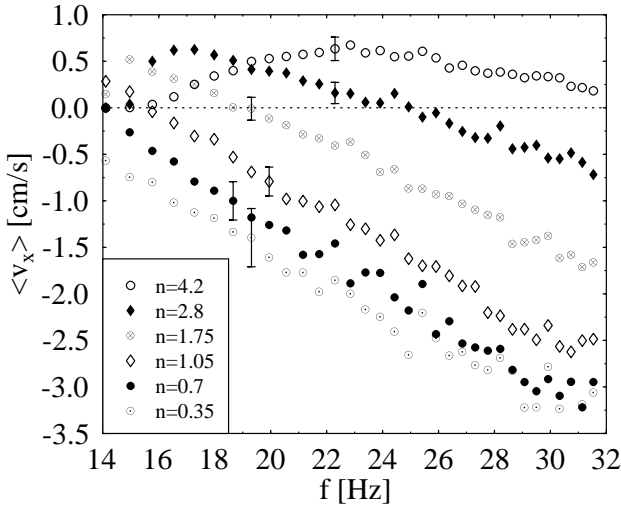


FIG. 10. Horizontal transport as a function of driving frequency, with six different layer widths. The shape of the sawtooth: $h = 6$ mm, $a = 0.25$. The system width is $10w = 60$ mm, one run lasted for 30 internal seconds. The plots for $n = 0.35$, $n = 0.7$, $n = 1.05$, $n = 1.75$, $n = 2.8$, and $n = 4.2$ are average of 30, 18, 12, 7, 7, 7 runs, respectively.

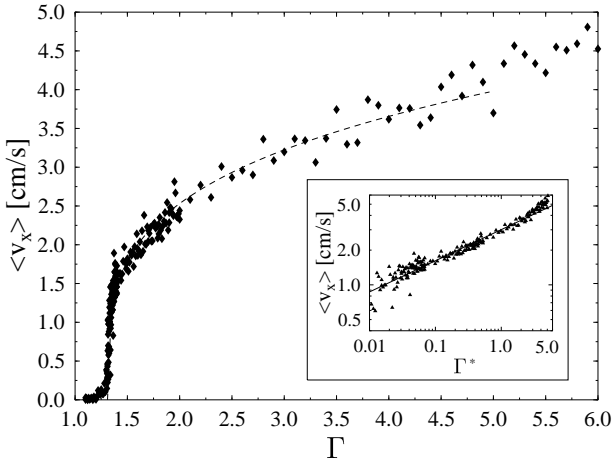


FIG. 11. Horizontal velocity $\langle v_x \rangle$ as a function of Γ . The shape of a sawtooth: $h = 3$ mm, $a = 0.1$. The layer width was $n = 0.7$, the system width $10w = 60$ mm. The simulations ran for 30 internal seconds. A power law function was fitted: $\Gamma^{*\gamma}$ with $\Gamma^* = (\Gamma - \Gamma_c)/\Gamma_c$. The fitted values are $\Gamma_c = 1.31 \pm 0.03$, and $\gamma = 0.27 \pm 0.05$.

D. Phase transition

When the driving frequency is not high enough (i.e., the dimensionless acceleration $\Gamma < 1$), then $\langle v_x \rangle = 0$, since the whole granular layer has zero velocity compared with the oscillating base (solid phase). However, the transport may remain zero for $\Gamma > 1$, until a critical acceleration. Increasing the frequency, some of the particles, and later all of them are flying (fluidized phase), therefore, transport may appear. We investigated this phase transition

(with control parameter $\langle v_x \rangle$) in case of two different sawtooth shapes. First we chose a shape which produces positive transport for a few particles. Figure 11 shows the Γ dependence of the velocity. The transport appears when $\Gamma > \Gamma_c = 1.31$. Above this, a power law of the form $\langle v_x \rangle \sim (\Gamma - \Gamma_c)^{0.27}$ can be fitted to the results.

Choosing a sawtooth for which the transport velocity is negative for small particle number, one expects different behavior. Fig. 12 shows how velocity depends on the frequency in such a case. The velocity becomes positive linearly above the critical frequency, and increasing the frequency, it turns back, and the transport reverses.

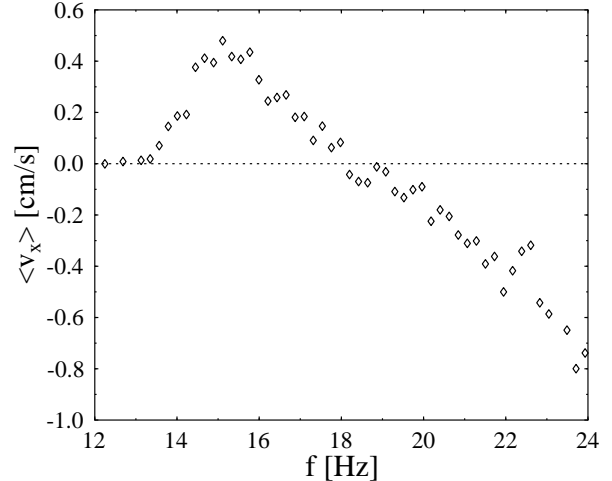


FIG. 12. Horizontal transport velocity as a function of driving frequency. The shape of a sawtooth: $h = 6$ mm, $a = 0.25$. The layer width is $n = 1.75$. The system width is $10w = 60$ mm, the simulations ran for 30 internal seconds.

V. DISCUSSION

According to our studies of a simplified geometrical model the following qualitative argument can be used to explain the observed current reversal as a function of the particle number: There is an intermediate size and asymmetry of the teeth for which a single ball falling from a range of near-vertical angles bounces back to the left (negative direction) in most of the cases. This effect is enhanced by rotation, due to friction between the ball and the tooth. However, if there are many particles present, this mechanism is destroyed, and on average, the direction of the motion of particles will become positive (the “natural” direction for this geometry); this corresponds to the usual ratcheting mechanism characterized by larger distances traveled by the particles along the smaller slope with occasional jumps over to the next valley between the teeth [9–12,23]. There is no net current for symmetric teeth in our case, however the motion of a single particle is very interesting in that situation as well [22].

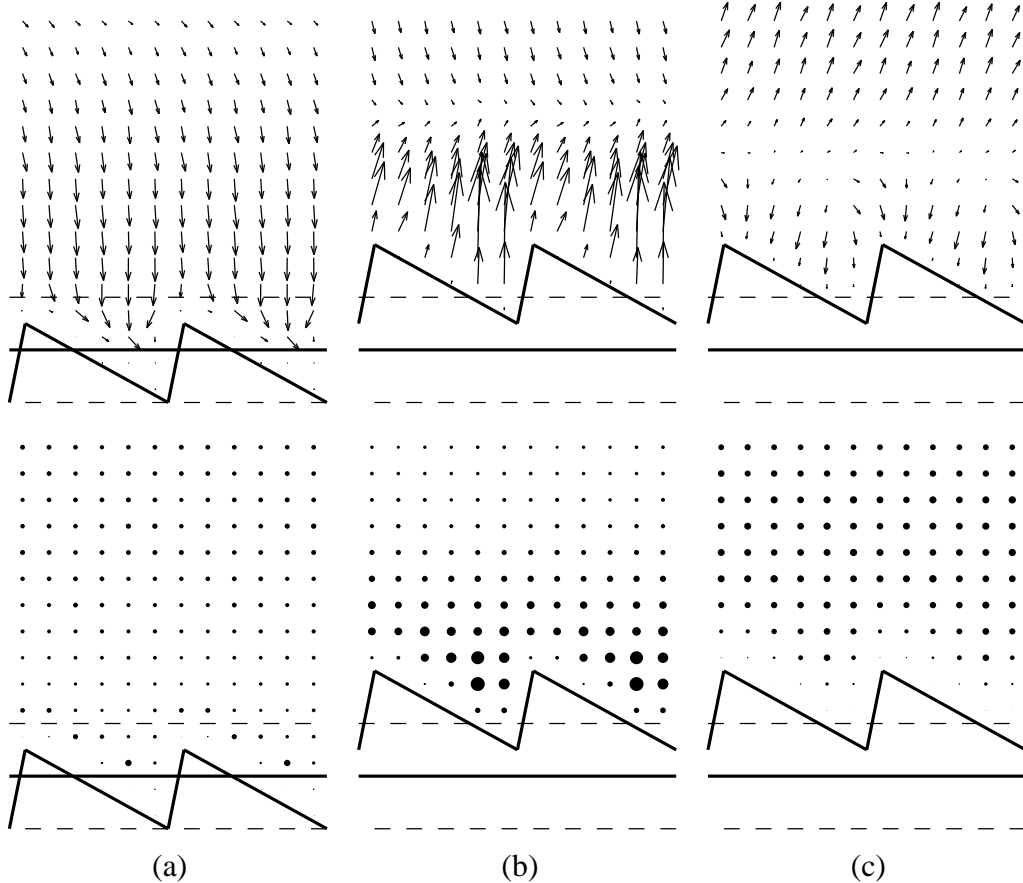


FIG. 13. Momentum density field (upper row) and mass density field (lower row) in case of *positive* horizontal transport ($\langle v_x \rangle = 3.9 \pm 0.3$ cm/s, $h = 3$ mm, $a = 0.1$, $f = 25$ Hz, $n = 0.7$). The arrows represent the average momentum vector in a box (with width $w/6$) starting from the center of the box, the radii of the disks are proportional to the average mass. (The momentum and mass carried by a particle whose center is in the box are taken into account when calculating the average in the box.) The momentum and the mass are averaged for these spatial boxes and phase frames of the oscillation (with length $2\pi/6$). In the j th frame, the phase $\phi = 2\pi ft$ of oscillation $A \sin(2\pi ft)$ is $j2\pi/6 \leq \phi < (j+1)2\pi/6$. (a) $j = 4$, (b) $j = 0$, (c) $j = 2$. The actual height of the simulation cell is three times larger than shown here.

The reversal of the current as a function of the frequency can be interpreted in a similar manner. For smaller frequencies there are many particles close to the base and the current is positive. For larger frequencies the granular state is highly fluidized, the density considerably decays and the mechanism leading to negative transport for a small number of particles (discussed above) comes into play.

To obtain a deeper insight into the process of horizontal flow, the momentum density field and mass distribution is plotted in case of *positive* (Fig. 13) and *negative* (Fig. 14) transport. In Fig. 13 it can be seen that the particles slide down the side with the smaller slope, and when the base is in rising phase, they are given a positive net horizontal impulse. It is worth noting that most particles do not collide with the opposite side. On the other hand, if the sawteeth are higher and more symmetric, the off-bouncing particles collide with the opposite side of the sawtooth, therefore their horizontal impulse is reversed, and the net current becomes negative (see Fig. 14).

We interpret the existence of maxima in Fig. 2 as a

function of the particle number as follows: If only a few particles are present, their motion is erratic, with large jumps in random directions. As the number of particles is increased, due to an inelastic collapse-like process, the particles start to move coherently, and this more ordered motion, together with the right frequency, seems to give rise to a kind of resonant behavior as far as transport is concerned. Similar maxima can also be observed in molecular motor calculations and simulations. Thick layers move more slowly because of inelastic damping.

The remarkable result that emerges from both experiment and simulation is that the flow direction can change as the layer thickness varies. This is entirely unexpected and requires further investigation; the only related behavior of which we are aware is the alternating current direction in a model of collectively moving interacting Brownian particles in a “flashing” ratchet potential [13].

In conclusion, we have investigated granular transport in a system inspired by models of molecular motors and have observed, both experimentally and numerically, that the behavior depends in a complex manner on the param-

eters characterizing the system. These results ought to stimulate further research into this fascinating class of

problems.

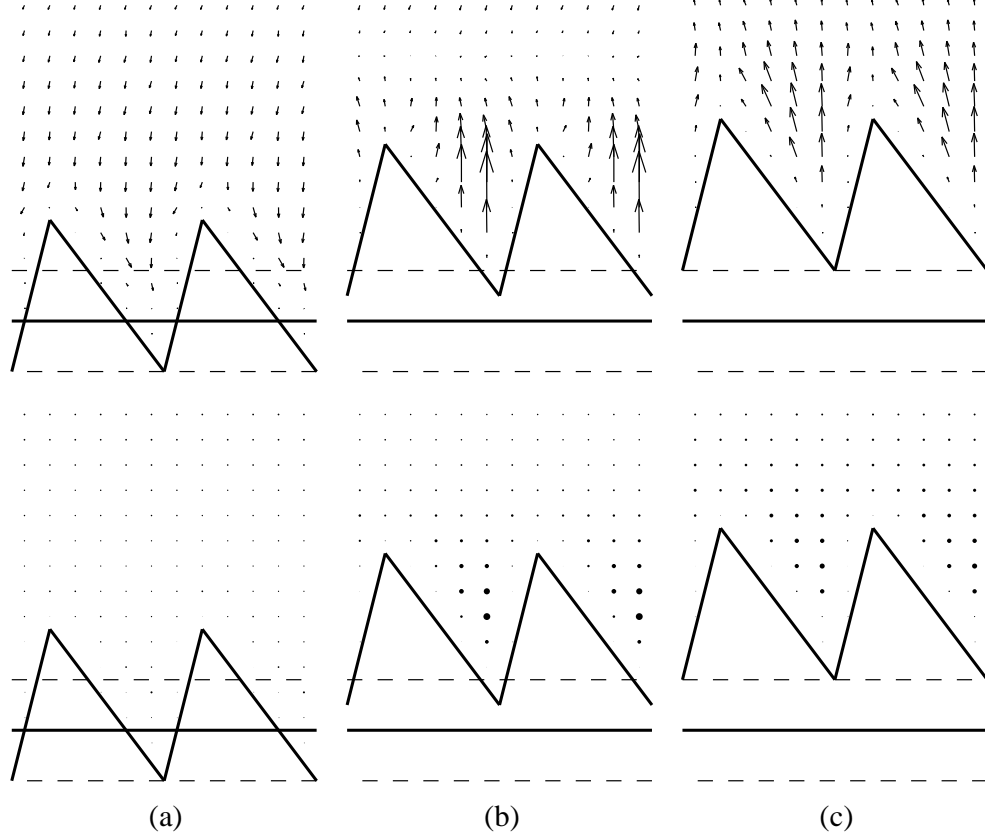


FIG. 14. The same as in Fig. 13, but in case of *negative* horizontal transport ($\langle v_x \rangle = -3.2 \pm 0.3$ cm/s, $h = 6$ mm, $a = 0.25$, $f = 30$ Hz, $n = 0.35$). (a) $j = 4$, (b) $j = 0$, (c) $j = 1$. The ratio of the absolute value of the average momentum in a box and the length of the arrow is the same as in Fig. 13.

ACKNOWLEDGEMENTS

Useful discussions with I. Derényi are acknowledged. One of the authors (T. V.) has had extensive interactions with D. Rapaport about the standard (not event driven) simulations of the present system (to be published). This work was supported in part by the Hungarian Research Foundation Grant No. T019299.

APPENDIX A: COLLISION MODEL

In event driven simulations the collisions are instantaneous, the final velocities are calculated from the initial ones.

To introduce our notation, let us have a look at Fig. 15. When two particles collide, the reference frame is fixed to the center of mass. The center of particle 1 is at \mathbf{r}_1 , and that of particle 2 is at \mathbf{r}_2 . The velocities and the angular velocities before the collision are \mathbf{v}_1 , \mathbf{v}_2 and ω_1 , ω_2 . The normal vector of the collision is $\mathbf{n} = \frac{\mathbf{r}_2 - \mathbf{r}_1}{|\mathbf{r}_2 - \mathbf{r}_1|}$,

and the tangential vector \mathbf{t} is obtained by rotating \mathbf{n} by 90° counter-clockwise. These two vectors define a local reference frame, and it is convenient to decompose all vectors into normal and tangential components.

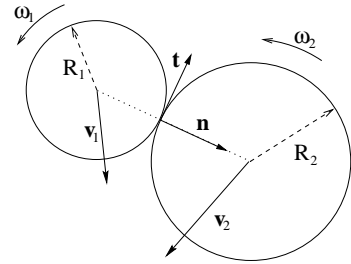


FIG. 15. Collision of two particles. The line connecting the centers of the particles defines a local coordinate system.

The relative normal velocity is

$$v_n = (\mathbf{v}_1 - \mathbf{v}_2) \cdot \mathbf{n} = v_{n1} - v_{n2}, \quad (A1)$$

and the relative tangential velocity is

$$v_t = (\mathbf{v}_1 - \mathbf{v}_2) \cdot \mathbf{t} = v_{t1} - v_{t2}. \quad (\text{A2})$$

It is useful to introduce other velocities, too. First, v_c , the sum of the circumferential velocities:

$$v_c = R_1\omega_1 + R_2\omega_2, \quad (\text{A3})$$

and second, v_r , the relative tangential velocities of the surfaces where the two particles touch each other:

$$v_r = v_t + v_c. \quad (\text{A4})$$

This velocity has two components: the first comes from the particles' translational movement, and the second from the rotation around their axis.

To characterize the dynamics of a collision, we use the simplest mechanical model of dissipation: the reduction of the relative normal velocity is described by ε_n , the velocity independent coefficient of restitution:

$$\varepsilon_n = -\frac{v'_n}{v_n} \quad (\text{A5})$$

(we use prime to denote quantities after collision). The Coulomb friction model is used for describing the tangential friction forces.

The normal component of the total momentum is zero in our reference frame:

$$m_1 v'_{n1} + m_2 v'_{n2} = 0. \quad (\text{A6})$$

Introducing $m_{\text{eff}} = \frac{m_1 m_2}{m_1 + m_2}$, the effective mass, from (A5) and (A6) we get

$$v'_{n1} = -\varepsilon_n \frac{m_{\text{eff}}}{m_1} v_n \quad (\text{A7})$$

and

$$v'_{n2} = \varepsilon_n \frac{m_{\text{eff}}}{m_2} v_n. \quad (\text{A8})$$

Let us denote the momentum transferred by particle 2 to particle 1 during the collision by \mathbf{J} . Then

$$m_1(v'_{n1} - v_{n1}) = J_n, \quad (\text{A9})$$

$$m_2(v'_{n2} - v_{n2}) = -J_n. \quad (\text{A10})$$

From (A9) and (A10), using (A5) we obtain:

$$J_n = -m_{\text{eff}} v_n (1 + \varepsilon_n). \quad (\text{A11})$$

From now on we have to distinguish between two cases: i) the particles are sliding on each other during the whole collision, and ii) the surfaces stick to each other at some time during the collision. In the latter case the result does not depend on when the surfaces stick to each other.

1. Sliding case

In this case the sliding friction force is acting on the particles. The absolute value of this force is μ times the normal force, its direction is tangential and opposite to the relative velocity of the sliding surfaces. Therefore the change of the particles' tangential momenta are:

$$m_1(v'_{1t} - v_{1t}) = \mu J_n \text{sign}(v_r), \quad (\text{A12})$$

$$m_2(v'_{2t} - v_{2t}) = -\mu J_n \text{sign}(v_r), \quad (\text{A13})$$

the change of the angular velocities are:

$$\Theta_1(\omega'_1 - \omega_1) = \mu R_1 J_n \text{sign}(v_r), \quad (\text{A14})$$

$$\Theta_2(\omega'_2 - \omega_2) = \mu R_2 J_n \text{sign}(v_r). \quad (\text{A15})$$

Let us write the moment of inertia in a general form $\Theta = lmR^2$. For example, if the particle is a disk, then $l = \frac{1}{2}$, if it is a ball, then $l = \frac{5}{2}$. From Eqs. (A12–A15) the velocities and angular velocities after the collision can be calculated easily:

$$\begin{aligned} v'_{1t} &= v_{1t} + \frac{\mu}{m_1} J_n \text{sign}(v_r) \\ &= v_{1t} - \mu(1 + \varepsilon_n) \frac{m_{\text{eff}}}{m_1} v_n \text{sign}(v_r) \end{aligned} \quad (\text{A16})$$

$$\begin{aligned} v'_{2t} &= v_{2t} - \frac{\mu}{m_2} J_n \text{sign}(v_r) \\ &= v_{2t} + \mu(1 + \varepsilon_n) \frac{m_{\text{eff}}}{m_2} v_n \text{sign}(v_r) \end{aligned} \quad (\text{A17})$$

$$\begin{aligned} R_1\omega'_1 &= R_1\omega_1 + \frac{\mu}{lm_1} J_n \text{sign}(v_r) \\ &= R_1\omega_1 - \frac{\mu(1 + \varepsilon_n)}{l} \frac{m_{\text{eff}}}{m_1} v_n \text{sign}(v_r) \end{aligned} \quad (\text{A18})$$

$$\begin{aligned} R_2\omega'_2 &= R_2\omega_2 + \frac{\mu}{lm_2} J_n \text{sign}(v_r) \\ &= R_2\omega_2 - \frac{\mu(1 + \varepsilon_n)}{l} \frac{m_{\text{eff}}}{m_2} v_n \text{sign}(v_r). \end{aligned} \quad (\text{A19})$$

2. Sticking case

In this case at some time during the collision the frictional force stops the rotation of the two particles, and after this their surfaces roll without sliding on each other. Translated into geometry this means:

$$v'_{t1} - v'_{t2} + R_1\omega'_1 + R_2\omega'_2 = 0. \quad (\text{A20})$$

Altough we do not know the exact sticking frictional force, we can say that the same force is acting in the tangential direction on the two particles:

$$\Theta_1(\omega'_1 - \omega_1) = R_1 m_1 (v'_{1t} - v_{1t}), \quad (\text{A21})$$

$$\Theta_2(\omega'_2 - \omega_2) = -R_2 m_2 (v'_{2t} - v_{2t}). \quad (\text{A22})$$

Using that the total momentum remains zero in the reference frame fixed to the center of mass, from Eqs. (A20–A22) we get:

$$v'_{1t} = \frac{1}{l+1}v_{1t} - \frac{l}{l+1}\frac{m_{\text{eff}}}{m_1}(R_1\omega_1 + R_2\omega_2) \quad (\text{A23})$$

$$v'_{2t} = \frac{1}{l+1}v_{2t} + \frac{l}{l+1}\frac{m_{\text{eff}}}{m_2}(R_1\omega_1 + R_2\omega_2) \quad (\text{A24})$$

$$\begin{aligned} R_1\omega'_1 &= R_1\omega_1\left(\frac{l}{l+1} + \frac{m_{\text{eff}}}{(l+1)m_2}\right) \\ &\quad - R_2\omega_2\frac{m_{\text{eff}}}{(l+1)m_1} - \frac{1}{l+1}v_{1t} \end{aligned} \quad (\text{A25})$$

$$\begin{aligned} R_2\omega'_2 &= R_2\omega_2\left(\frac{l}{l+1} + \frac{m_{\text{eff}}}{(l+1)m_1}\right) \\ &\quad - R_1\omega_1\frac{m_{\text{eff}}}{(l+1)m_2} + \frac{1}{l+1}v_{2t}. \end{aligned} \quad (\text{A26})$$

3. The condition for sticking or sliding

Now let us investigate the case when the surfaces of the particles are sliding on or stick to each other during the collision. As the frictional force acts, the relative velocity of the touching surfaces decreases, and they stick to each other if this velocity becomes zero. Expressing the relative velocity of the surfaces after the collision from Eqs. (A16–A19) we get

$$\begin{aligned} v'_r &= v'_{1t} - v'_{2t} + R_1\omega'_1 + R_2\omega'_2 \\ &= v_r - \frac{l+1}{l}\mu(1+\varepsilon_n)v_n\text{sign}(v_r). \end{aligned} \quad (\text{A27})$$

From this it follows that the surfaces are sliding on each other during the whole collision if and only if

$$\frac{|v_r|}{v_n} \geq \frac{l+1}{l}\mu(1+\varepsilon_n), \quad (\text{A28})$$

otherwise they are sticking before the end of the collision, and results (A23–A26) are valid.

4. Particle collides with wall

When a particle collides with the wall, then the latter can be regarded as another particle with an infinite mass, so all of our results for binary collisions can be used. The only task remaining is to replace the effective mass with the mass of the colliding particle.

5. Collision operator

The collision operator makes connection between the velocities before and after collision. If we introduce a

velocity “vector” \mathbf{w} , which includes the relative normal (v_n), tangential (v_t) and circumferential velocity v_c :

$$\mathbf{w} = (v_n, v_r, v_c), \quad (\text{A29})$$

then the velocity after the collision (\mathbf{w}') is determined from the initial velocity (\mathbf{w}) by a matrix (\mathbf{C}) with 3×3 components:

$$\mathbf{w}' = \mathbf{C}\mathbf{w}. \quad (\text{A30})$$

This matrix represents the collision operator. In our case we can write the collision matrix for the sliding case from Eqs. (A16–A19):

$$\mathbf{C}^{\text{sl}} = \begin{pmatrix} -\varepsilon_n & 0 & 0 \\ -\mu(1+\varepsilon_n)\text{sign}(v_r) & 1 & 0 \\ -\frac{\mu(1+\varepsilon_n)}{l}\text{sign}(v_r) & 0 & 1 \end{pmatrix} \quad (\text{A31})$$

and from Eqs. (A23–A26) for the sticking case:

$$\mathbf{C}^{\text{st}} = \begin{pmatrix} -\varepsilon_n & 0 & 0 \\ 0 & \frac{1}{l+1} & -\frac{l}{l+1} \\ 0 & -\frac{1}{l+1} & \frac{l}{l+1} \end{pmatrix}. \quad (\text{A32})$$

APPENDIX B: COLLISIONS AS EVENTS

In an event driven algorithm the pace of the simulation is determined by the time sequences between collisions. There are four types of collisions, i.e., a particle may collide with a (i) particle, (ii) resting segment, (iii) oscillating segment, and (iv) oscillating arc. To find the next collision is the heart of the matter. One has to calculate the times of the possible collisions and find the closest one. Let us assume that the last collision occurred at $t = 0$, therefore positive time values correspond to the future, negative values to the past. Now we show the calculation of the collision time in full detail in all cases.

1. Particle–particle collision

The motion of particle i until its next collision in a gravitational field is determined by its position \mathbf{r}_{0i} and velocity \mathbf{v}_{0i} at time t_i . As the two particles (1 and 2) are moving along parabolic paths, their position at time t are

$$\mathbf{r}_1(t) = \mathbf{r}_{01} + \mathbf{v}_{01}(t - t_1) - \mathbf{j}\frac{g}{2}(t - t_1)^2 \quad (\text{B1})$$

$$\mathbf{r}_2(t) = \mathbf{r}_{02} + \mathbf{v}_{02}(t - t_2) - \mathbf{j}\frac{g}{2}(t - t_2)^2, \quad (\text{B2})$$

where \mathbf{j} is a unit vector having opposite direction to that of gravity. A collision occurs if $|\mathbf{r}_1(t) - \mathbf{r}_2(t)| = R_1 + R_2$, which can be written, using (B1–B2) and introducing the following notations

$$\mathbf{p} = \mathbf{v}_{01} - \mathbf{v}_{02} + \mathbf{j}g(t_1 - t_2)$$

$$\mathbf{q} = \mathbf{r}_{01} - \mathbf{r}_{02} + \mathbf{v}_{02}t_2 - \mathbf{v}_{01}t_1 - \mathbf{j}\frac{g}{2}(t_1^2 - t_2^2)$$

as

$$|\mathbf{p}t + \mathbf{q}| = R_1 + R_2. \quad (\text{B3})$$

Taking the square of (B3) and divide it by 2 we get

$$\frac{\mathbf{p}^2}{2}t^2 + \mathbf{p} \cdot \mathbf{q}t + \frac{\mathbf{q}^2 - (R_1 + R_2)^2}{2} = 0. \quad (\text{B4})$$

The two particles can collide with each other only if $|\mathbf{p}| \neq 0$ and

$$D = (\mathbf{p} \cdot \mathbf{q})^2 - \mathbf{p}^2(\mathbf{q}^2 - (R_1 + R_2)^2) \quad (\text{B5})$$

is nonnegative, otherwise the particles will not collide. If $D > 0$, then the two times when the condition of touching is fulfilled are

$$t_{1,2}^{\text{coll}} = \frac{-\mathbf{p} \cdot \mathbf{q} \pm \sqrt{D}}{\mathbf{p}^2}, \quad (\text{B6})$$

where $t_1^{\text{coll}} < t_2^{\text{coll}}$. (If $D = 0$, then $t_1^{\text{coll}} = t_2^{\text{coll}}$, and this means that the two particles only touch each other, so we may consider that no collision occurs in this case.) Since the smaller solution gives the time of the first touching, and only collisions in the future should be regarded, the actual time of the collision is given by t_1^{coll} if $t_1^{\text{coll}} > 0$, otherwise no collision occurs. Summarizing the results, two particles collide, and then the collision time is t_1^{coll} , if and only if all of the following three conditions are fulfilled: $|\mathbf{p}| \neq 0$, $D > 0$, and $t_1^{\text{coll}} > 0$.

2. Particle–resting segment collision

Let us denote the position and the velocity of the particle by \mathbf{r}_0 and \mathbf{v}_0 respectively at time t_0 . Let \mathbf{n} be a unit vector perpendicular to the segment, pointing towards the inside of the simulation space, and \mathbf{s}_1 and \mathbf{s}_2 the left and right side end point of the segment with respect to \mathbf{n} (see Fig. 16).

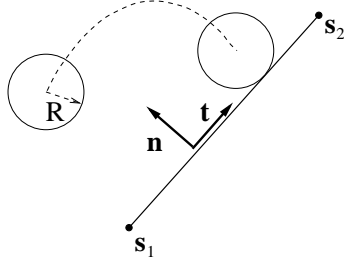


FIG. 16. Particle colliding with a resting segment. The particle arrives from the inside of the simulation space and collides with the segment between its ending points \mathbf{s}_1 and \mathbf{s}_2 .

Since the particle is moving along a parabolic path in the gravitational field, its position as a function of time is

$$\mathbf{r}(t) = \mathbf{r}_0 + \mathbf{v}_0(t - t_0) - \mathbf{j}\frac{g}{2}(t - t_0)^2, \quad (\text{B7})$$

while its speed is

$$\mathbf{v}(t) = \mathbf{v}_0 - \mathbf{j}g(t - t_0). \quad (\text{B8})$$

The particle collides with the line if

$$(\mathbf{r}(t) - \mathbf{s}_1) \cdot \mathbf{n} = R, \quad (\text{B9})$$

which, after inserting $\mathbf{r}(t)$ from (B7) and using the following notations:

$$u = -\frac{g}{2}\mathbf{j} \cdot \mathbf{n}, \quad v = (\mathbf{j}gt_0 + \mathbf{v}_0) \cdot \mathbf{n},$$

$$w = (\mathbf{r}_0 - \mathbf{s}_1 - \mathbf{v}_0t_0 - \mathbf{j}\frac{g}{2}t_0^2) \cdot \mathbf{n} - R, \quad D = v^2 - 4uv$$

can be written as

$$ut^2 + vt + w = 0. \quad (\text{B10})$$

We have to consider several cases. First, if $u = 0$ (in other words \mathbf{j} and \mathbf{n} are perpendicular to each other, therefore the segment is vertical), then at most one solution is possible. If $v = 0$ in this case, we can say that no collision occurs. If $v \neq 0$, the solution is

$$t_0^{\text{coll}} = -\frac{w}{v}, \quad (\text{B11})$$

and this is valid only if $t_0^{\text{coll}} \geq 0$. If $u \neq 0$, then, provided that $D > 0$, there are different solutions:

$$t_{1,2}^{\text{coll}} = \frac{-v \pm \sqrt{D}}{2u}. \quad (\text{B12})$$

If $D \leq 0$, then we have either one (the particle just touches the line) or no solution. In these cases no collision occurs. Now let us assume that (B10) has one or more solutions, which can be t_0^{coll} , t_1^{coll} , or t_2^{coll} . Nevertheless, two more conditions have to be fulfilled at the same time:

- (i) at the moment of collision the particle has to come from the inside of the simulation space, i.e.,

$$\mathbf{v}(t^{\text{coll}}) \cdot \mathbf{n} < 0, \quad (\text{B13})$$

where t^{coll} denotes a solution. It is clear that even if there are two solutions, after (B13) only one remains.

- (ii) It is not enough to collide with the line of the segment, the particle has to collide with it between its ending points \mathbf{s}_1 and \mathbf{s}_2 . This is true if

$$(\mathbf{r}(t^{\text{coll}}) - \mathbf{s}_1) \cdot \mathbf{t} \geq 0 \quad \text{and} \quad (\mathbf{r}(t^{\text{coll}}) - \mathbf{s}_2) \cdot \mathbf{t} \leq 0, \quad (\text{B14})$$

where $\mathbf{t} = \frac{\mathbf{s}_2 - \mathbf{s}_1}{|\mathbf{s}_2 - \mathbf{s}_1|}$, a unit vector parallel to the segment. Summarizing, a particle collides with a segment only if (B10) has solution, and with this solution both (i) and (ii) conditions are fulfilled.

3. Particle–oscillating segment collision

In this case the time of collision cannot be obtained in a closed form, a numerical method has to be used. The segment (and so its left ending point) is oscillating in vertical direction:

$$\mathbf{s}_1(t) = \mathbf{s}_{10} + \mathbf{j}A \sin(2\pi ft + \phi_0) \quad (B15)$$

Let the particle has the same properties as in the previous (particle-resting segment collision) case. Then we get the equation for collision by replacing \mathbf{s}_1 by $\mathbf{s}_1(t)$ in (B9). We can assume that $\mathbf{j}\mathbf{n} \neq 0$, so the segment is not vertical (if it is, then with a slight modification it can be taken as a resting segment). Using the notations

$$u = -\frac{g}{2A}, \quad b = \frac{(\mathbf{j}gt_0 + \mathbf{v}_0) \cdot \mathbf{n}}{A\mathbf{j} \cdot \mathbf{n}},$$

$$w = \frac{(2\mathbf{r}_0 - 2\mathbf{s}_{10} - 2\mathbf{v}_0 t_0 - \mathbf{j}gt_0^2) \cdot \mathbf{n}}{2A\mathbf{j} \cdot \mathbf{n}},$$

the equation is

$$ut^2 + vt + w = A \sin(2\pi ft + \phi_0). \quad (B16)$$

This equation can be solved only numerically. First, we have to find the time region in which a solution is possible.

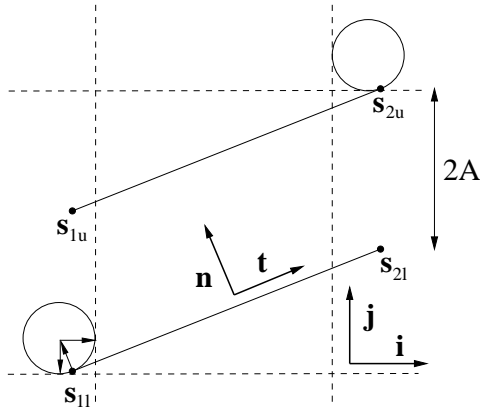


FIG. 17. A particle can collide with an oscillating segment only if it enters the area bounded by the two vertical dashed lines and its lowest point is between the two horizontal dashed lines.

In Fig. 17 one can see the segment in the lowest and the highest positions, and two particles touching the segment at its left end point \mathbf{s}_{1l} (in the lowest position) and right end point \mathbf{s}_{2u} (in the highest position). It is easy to see that the particle can collide with the segment if (i) it enters the area bounded by the two vertical dashed lines and (ii) the particle's lowest point is in the area bounded by the two horizontal dashed lines. Regarding these dashed lines as resting segments, using our previous results, we can determine the time intervals T_v and T_h

when the particle is in a position that conditions (i) and (ii) are fulfilled. For this, one point of each of these segments has to be determined (as their direction is known). The center of the particle touching the segment at point \mathbf{s}_{1l} is at point $\mathbf{s}_{1l} + R\mathbf{n}$, so one point of the vertical boundary line is $\mathbf{s}_{1l} + R\mathbf{n} + R(\mathbf{j} \cdot \mathbf{n})\mathbf{i}$, and that of the horizontal boundary line is $\mathbf{s}_{1l} + R\mathbf{n} - R(\mathbf{j} \cdot \mathbf{n})\mathbf{j}$. Similarly, for point \mathbf{s}_{2u} , these are $\mathbf{s}_{2u} + R\mathbf{n} - R(\mathbf{j} \cdot \mathbf{n})\mathbf{i}$ and $\mathbf{s}_{2u} + R\mathbf{n} - R(\mathbf{j} \cdot \mathbf{n})\mathbf{j}$, respectively. The dot product $\mathbf{j}\mathbf{n}$ is needed to ensure the validity of our results if \mathbf{n} is pointing downwards. (In this case ‘left’ and ‘right’, and ‘up’ and ‘down’ also have to be swapped.) The time interval T_v , when the particle is between the vertical dashed lines, is a closed interval (in a special case, when the particle is moving vertically, this can include all time). The time interval T_h , while the lowest point of the particle is between the horizontal dashed lines, can be empty or one closed interval or two disjunctive closed intervals. Furthermore, only solutions in the future are valid, i.e., a solution has to fall into the time interval $T_* = [t_*, \infty[$. Summarizing, a particle collides with a segment if (B16) has solution in the time interval $T = T_h \cap T_v \cap T_*$, and if there are more than one of them, the smallest one is the time of collision. In our simulation the *bisection method* [30] was used, with ending tolerance 10^{-12} s.

4. Particle–oscillating circle collision

The method of finding the collision time is similar to that of in the previous case. The center of the circle is moving according to

$$\mathbf{s}(t) = \mathbf{s}_0 + \mathbf{j}A \sin(2\pi ft + \phi_0) \quad (B17)$$

(see Fig. 18).

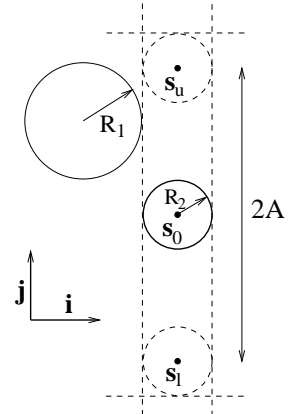


FIG. 18. A particle can collide with an oscillating circle only if it enters the rectangular area bounded by the two vertical dashed lines and the two horizontal dashed lines.

The particle with radius R_1 is moving again along a parabolic path, its position is given by (B7). The equation for the collision time is

$$|\mathbf{r}(t) - \mathbf{s}(t)| = R_1 + R_2, \quad (\text{B18})$$

where R_2 is the radius of the circle. It is a transcendental equation, and we use again the bisection method for solving it. The collision may occur only if the the particle enters the rectangular area bounded by the two horizontal and vertical lines in Fig. 18. It is easy to determine these lines: the horizontal lines contain points $\mathbf{s}_l - R_2\mathbf{j}$ and $\mathbf{s}_u + R_2\mathbf{j}$, while the vertical lines contain points $\mathbf{s}_0 \pm R_2\mathbf{i}$. The time region of possible collision can be calculated similarly to the case of particle–oscillating segment collision.

- [10] M. O. Magnasco, Phys. Rev. Lett. **71**, 1477 (1993).
- [11] R. D. Astumian and M. Bier, Phys. Rev. Lett. **72**, 1766 (1994)
- [12] C. R. Doering, W. Horsthemke, and J. Riordan, Phys. Rev. Lett. **72**, 2984 (1994).
- [13] I. Derényi and A. Ajdari, Phys. Rev. E **54**, R5 (1996).
- [14] I. Derényi and T. Vicsek, Phys. Rev. Lett. **75**, 374 (1995).
- [15] F. Jülicher and J. Prost, Phys. Rev. Lett. **75**, 2618 (1995).
- [16] M. Nakagawa, S. A. Altobelli, A. Caprhan, E. Fukushima, and E-K. Jeong, Exp. Fluids **16**, 54 (1993).
- [17] J. A. C. Gallas, H. J. Herrmann, and S. Sokolowski, J. Phys. (France) II **2**, 1389 (1992).
- [18] I. Derényi, P. Tegzes, and T. Vicsek *Chaos* **8** 657 (1998).
- [19] P. Bergé and M. Dubois, Contemp. Phys. **25**, 535 (1984).
- [20] G. C. Barker, in *Granular Matter: An Interdisciplinary Approach*, edited by A. Mehta (Springer, Heidelberg, 1994), p. 35.
- [21] H. J. Herrmann, in *3rd Granada Lectures in Computational Physics*, edited by P. L. Garrido and J. Marro (Springer, Heidelberg, 1995), p. 67.
- [22] J. Duran, Europhys. Lett., **17**, 679 (1992)
- [23] A. L. R. Bug and B. J. Berne Phys. Rev. Lett. **59**, 948 (1987)
- [24] M. P. Allen and D. J. Tildesley, *Computer Simulation of Liquids* (Clarendon Press, Oxford, 1987)
- [25] D. E. Wolf, in *Computational Physics: Selected Methods – Simple Exercises – Serious Applications*, edited by K. H. Hoffmann and M. Schreiber (Springer, Heidelberg, 1996), p. 64.
- [26] D. C. Rapaport, *The Art of Molecular Dynamics Simulation* (Cambridge University Press, Cambridge, 1995).
- [27] S. McNamara and W. R. Young, Phys. Fluids A **4**, 496 (1992).
- [28] S. Luding, E. Clément, J. Rajchenbach, and J. Duran, Europhys. Lett. **36**, 247 (1996).
- [29] Z. Farkas, Diploma thesis, Eötvös University, 1998.
- [30] W. H. Press, S. A. Teukolsky, W. T. Vetterling, and B. P. Flannery, *Numerical Recepies in C* (Cambridge University Press, Cambridge, 1992).